Effects of Imperfect Interface on the Dispersion Curves of Torsional Waves in a Composite Hollow Cylinder

JUNZHEN WANG and JIANMIN QU

ABSTRACT

This paper investigates the influence of interfacial imperfections on the dispersion relationship of torsional waves in a composite hollow cylinder. The imperfect interface between the inner and outer tubes is modelled by a linear spring interface model, where tractions are continuous across the interface and the displacement jump is assumed to be proportional to the tangential shear stress acting on the interface. The dispersion curves of normalized frequency as a function of normalized wavenumber can be determined by solving an eigenvalue problem. It is shown that for a fixed wavenumber, the modal frequency decreases with increasing interfacial spring compliance, especially for smaller wavenumbers. Besides, at larger wavenumbers, the loss of perfect continuity at the interface has a reduced impact. The thickness effect of the outer tube is further analyzed. The computational results indicate that the modal frequency rises in the case of the thinner coating layer. These torsional wave propagation features may provide insights and guidelines for nondestructive evaluation of composite hollow cylinders with imperfect interfaces. The paper finishes with a summary and concluding remarks.

INTRODUCTION

Hollow cylindrical structures are often deployed for heat and gas transportation purposes in aerospace and civil engineering. Such components usually consist of an inner and outer layer and are made of different isotropic or composite materials. However, during the in-service period, interfacial imperfections may take place due to the variation of stress distribution, leading to the emergence of damages, such as delamination and slippage. Therefore, it is of great importance to develop effective methodologies for interfacial damage detection in cylindrical structures before catastrophic failure occurs.

Junzhen Wang, Department of Mechanical Engineering, Stevens Institute of Technology, Hoboken, New Jersey 07030, USA, jwang13@stevens.edu.
Jianmin Qu, Department of Mechanical Engineering, Stevens Institute of Technology, Hoboken, New Jersey 07030, USA.

Torsional waves have been proven as a powerful candidate for the inspection of pipe-like structures, and their wave-propagation characteristics have also been extensively studied by the Non-destructive Evaluation (NDE) and Structural Health Monitoring (SHM) communities [1]-[4]. The classic linear three-dimensional theory of elasticity was employed to model the propagation of harmonic waves in composite cylinders. It can be noticed that the continuity conditions at the interface were further utilized since the interface between the layers was considered as perfect, i.e., continuity of displacement and traction. However, in practical applications, it is still hard to guarantee interfacial perfection even though adopting advanced welding technology for interface bonding. In addition, the interfacial imperfections may evolve into a more serious scenario and even endanger the integrity of the entire structure. Therefore, the investigation of the influence of imperfect interface on the torsional wave features becomes necessary and meaningful. Many researchers have spared efforts to investigate the dispersion curves of torsional waves in bi-material cylinders with imperfect interface conditions. Berger et al. modified the standard perfect-interface condition by introducing the displacement jump between the core and the cladding [5]. Based on this pioneer's work, the effect of the initial stresses on torsional wave dispersion curves was further studied [6, 7]. In this study, a composite hollow cylinder is considered, and it is assumed that the interface between the inner and outer tubes is imperfect.

This paper is arranged as follows. The spring interface model is initially formulated to introduce the interfacial imperfections into the frequency equation. The dispersion curves with varying imperfect interface conditions are then presented. Subsequently, the thickness effects of the outer tube are investigated and the computational results considering various coating thicknesses are discussed. Finally, some conclusions are given.

SPRING INTERFACE MODEL FORMULATION

Let (r,θ,z) be cylindrical polar coordinates. We consider a composite hollow cylinder shown in Figure 1. The cylinder consists of a hollow, $r<c$, an inner tube, $c<r<a$, and an outer tube, $a<r<b$. It is assumed that both tubes are made of linearly elastic materials, noted as material 1 and 2, respectively. The corresponding material properties and geometries of the cylinder are accordingly presented in TABLE I and TABLE II.

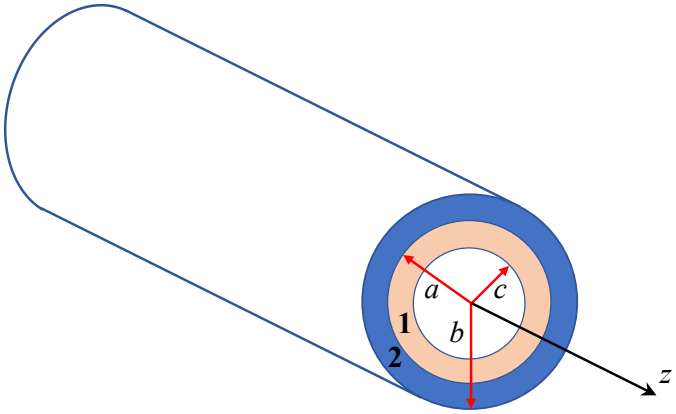

Figure 1. A composite hollow cylinder.

TABLE I. MATERIAL PROPERTIES OF THE CYLINDER

Materials	Young's modulus E (GPa)	Poisson's ratio υ	Density ρ (g/cm^3)
Material 1 (Zircaloy-4)	99.3	0.37	6.56
Material 2 (Chromium)	279	0.21	7.19

TABLE II. GEOMETRIES OF THE CYLINDER

Inner tube radius a (mm)	Outer tube radius b (mm)	Hollow radius c (mm)
11	11.1	10

For torsional waves, the only non-zero displacement component is the tangential displacement v, and v itself should be independent of θ. The governing equation in polar coordinates is given by [8]

$$\frac{\partial \sigma_{r\theta}}{\partial r}+\frac{2\sigma_{r\theta}}{r}+\frac{\partial \sigma_{\theta z}}{\partial z}=\rho\frac{\partial^2 v}{\partial t^2}. \tag{1}$$

Hooke's law relates the stresses $\sigma_{r\theta}$ and $\sigma_{\theta z}$ to v as

$$\sigma_{r\theta}=\mu\left(\frac{\partial v}{\partial r}-\frac{v}{r}\right) \text{ and } \sigma_{\theta z}=\mu\frac{\partial v}{\partial z}, \tag{2}$$

where μ represents the Lamé constant.

Making use of Eq. (2) into Eq. (1) gives

$$\frac{\partial^2 v}{\partial r^2}+\frac{1}{r}\frac{\partial v}{\partial r}-\frac{v}{r^2}+\frac{\partial^2 v}{\partial z^2}=\frac{1}{c^2}\frac{\partial^2 v}{\partial t^2}, \tag{3}$$

where $c^2=\sqrt{\mu/\rho}$ denotes the speed of shear waves in an infinite domain.

For waves propagating in the positive z-direction, which can be formulated as

$$v(r,z,t)=V(r)e^{i(kz-\omega t)}, \tag{4}$$

where i stands for $\sqrt{-1}$, k and ω are real. Then, substituting Eq. (4) into Eq. (3), which renders

$$\frac{d^2V}{dr^2}+\frac{1}{r}\frac{\partial V}{\partial r}+\left(\frac{\omega^2}{c^2}-k^2-\frac{1}{r^2}\right)V=0. \tag{5}$$

This is Bessel's function of order one. Its solutions depend on the sign of $\omega^2-k^2c^2$, which can be defined as

$$\begin{cases} Z_n=J_n, W_n=Y_n, q=\sqrt{(\omega/c)^2-k^2}, \omega^2>k^2c^2 \\ Z_n=(-1)^n I_n, W_n=K_n, q=\sqrt{k^2-(\omega/c)^2}, \omega^2<k^2c^2 \end{cases}, \tag{6}$$

where J_n and Y_n are Bessel functions and I_n and K_n are modified Bessel functions.

Thus, the appropriate solution of Eq. (5) takes the form of [5]

$$v=\left[q^{-1}AZ_1(qr)+qb^2BW_1(qr)\right]e^{i(kz-\omega t)}, \tag{7}$$

where A and B are arbitrary constants; $Z_0'(x)=-Z_1(x)$ and $W_0'(x)=-W_1(x)$. And we can use the expression above to indicate quantities in the inner and outer tubes with subscripts 1 and 2, respectively. The displacement can be expressed as

$$v(r,k)=\begin{cases}\left[q_1^{-1}A_1Z_1(q_1r)+q_1a^2B_1W_1(q_1r)\right]e^{i(kz-\omega t)}, c\le r\le a\\ \left[q_2^{-1}A_2Z_1(q_2r)+q_2b^2B_2W_1(q_2r)\right]e^{i(kz-\omega t)}, a\le r\le b\end{cases}, \quad (8)$$

where

$$q_j=\begin{cases}\sqrt{k_j^2-k^2}, k_j^2\ge k^2\\ \sqrt{k^2-k_j^2}, k_j^2\le k^2\end{cases}, j=1,2, \quad (9)$$

where $k_j=\omega/c_j$.

Boundary and Interface Conditions

With reference to Figure 1, now we need to enforce the boundary and interface conditions to the formulations. The traction-free boundary conditions should be applied on both inner and outer surfaces as

$$\sigma_{r\theta}(c)=0 \text{ and } \sigma_{r\theta}(b)=0. \quad (10)$$

The imperfect interface conditions often involve the distinction of displacements and tractions between the two contact surfaces [9]. And for most numerical models, these quantities on different sides of interfaces are assumed to be linearly related with each other. In this study, the imperfect interface is considered and modeled by a linear spring interface model. The interfacial tractions are continuous across the interface, and the displacement jump is proportional to the tangential shear stress acting on the surface. An interfacial spring compliance constant is introduced to represent the interfacial imperfections, denoted as γ . Therefore, the interface conditions can be illustrated as

$$\sigma_{r\theta}(a^+)=\sigma_{r\theta}(a^-) \quad (11)$$

and

$$v(a^+)-v(a^-)=\gamma a\frac{\sigma_{r\theta}(a)}{\mu_1}. \quad (12)$$

It should be noted that the perfect interface condition would be recovered when $\gamma=0$.

Frequency Equation for Dispersion Curves Calculation

The torsional wave dispersion curves can be determined by combining the displacement and stress equations with the boundary and interface conditions. Substituting Eq. (2) and Eq. (8) into Eq. (10), yields

$$A_1Z_2(q_1c)+(q_1a)^2B_1W_2(q_1c)=0, \quad (13)$$

$$A_2Z_2(q_2b)+(q_2b)^2B_2W_2(q_2b)=0. \quad (14)$$

From the continuity condition of traction from Eq. (11)

$$(\mu_1/\mu_2)\left[A_1Z_2(q_1a)+(q_1a)^2B_1W_2(q_1a)\right]-A_2Z_2(q_2a)-(q_2b)^2B_2W_2(q_2a)=0. \quad (15)$$

In terms of the displacement jump interface condition by Eq. (12), it turns out as

$$\begin{aligned}&(q_1b)^{-1}A_1\left[Z_1(q_1a)-\gamma q_1aZ_2(q_1a)\right]-(q_2b)^{-1}A_2Z_1(q_2a)\\&-(q_1b)^{-1}(q_1a)^2B_1\left[\gamma q_1aW_2(q_1a)-W_1(q_1a)\right]-B_2q_2bW_1(q_2a)=0\end{aligned}. \quad (16)$$

Eqs. (13)-(16) provide four equations in the four unknown constants, A_1, A_2, B_1, and

B_2 . In matrix form, the system of equation can be expressed as

$$\mathbf{Db} = \mathbf{0},\ \mathbf{b} = \left(A_1, A_2, B_1, B_2\right)^T. \tag{17}$$

Once the eigenvalue problem of Eq. (17) is solved, one will have the dispersion relationship between $k^{(n)}$ and k_1 or k_2, where $k^{(n)}$ is the eigenvalues of Eq. (17). Further, the eigenvector $\mathbf{b}$ can also be solved up to a constant amplitude. By normalizing it, one can have

$$\mathbf{b}^* \cdot \mathbf{b}^T = 1, \tag{18}$$

where the asterisk represents complex conjugate; the superscript *T* means the transpose operation. Note that all components of $\mathbf{b}$ are known in terms of material parameters, the given frequency ω, and the corresponding wavenumber k.

Finally, for a nontrivial solution, we can identify the frequency equation for dispersion curves calculation as

$$\det \mathbf{D} = 0. \tag{19}$$

We have determined the dispersion curves with normalized frequency,

$$\Omega_2 = k_2(b-a) \tag{20}$$

as a function of normalized axial wavenumber

$$\xi = k(b-a), \tag{21}$$

for a given value of the interfacial spring compliance constant γ.

DISPERSION CURVES WITH VARYING INTERFACE CONDITIONS

In this section, we will present the computational results considering different interface conditions., i.e., $\gamma = 0$, $\gamma = 0.1$, $\gamma = 0.5$, and $\gamma = 1$. Figure 2 shows the dispersion curves for the second mode and Figure 3 displays the third mode. It should be noted that the wave features of the first torsional mode are identical regardless of the interface conditions. The detailed demonstration can be found in Ref. [5]. With the increment of interface spring compliance, the modal frequency decreases dramatically, especially at the small values of wavenumber. On the other hand, the influence of interfacial imperfections fades when it comes to larger values of ξ as all the dispersion curves gradually convergence.

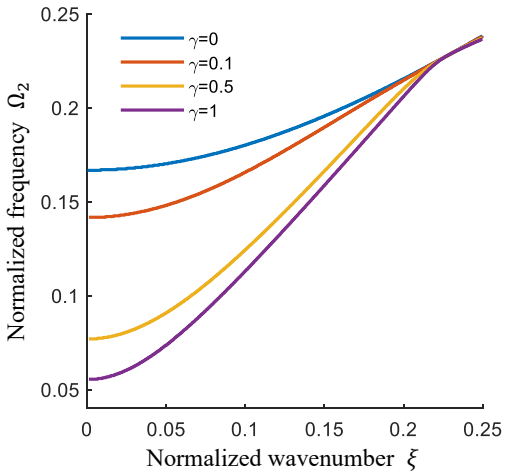

Figure 2. Dispersion curves for the second mode in a composite hollow cylinder.

The torsional waves for the third mode exhibit similar characteristics to the second mode. When the imperfect interface starts to emerge, the modal frequencies obviously drop in comparison with the perfect-interface case. It means that the variation of resonant frequencies of the third mode can serve as a competitive candidate to predict the appearance of interfacial imperfects. On the other hand, with the spring compliance continuing to increase, its influence on the resonant frequency fades. In addition, one corner at $\xi = 0.22$ can be noticed in the dispersion curve for $\gamma = 1$.

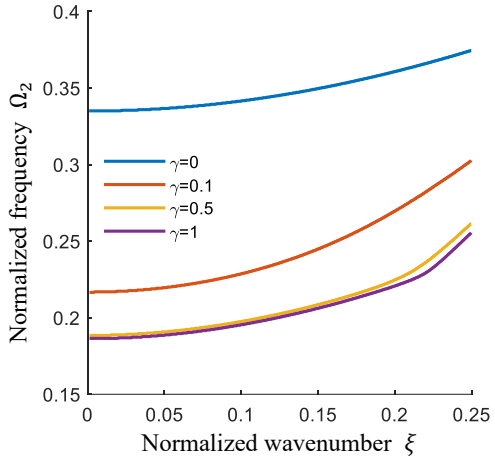

Figure 3. Dispersion curves for the third mode in a composite hollow cylinder.

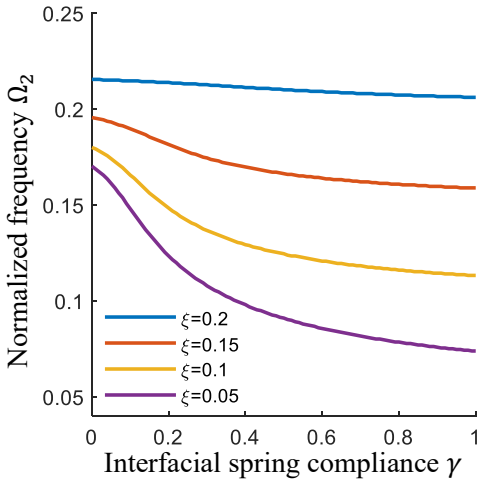

Figure 4. Normalized frequency VS interfacial spring compliance at fixed wavenumber for the second mode.

Another approach to determine the effects of imperfect interface is analyzing the dispersion curves with respect to interfacial spring compliance by fixed wavenumber. Figure 4 illustrates the numerical results for the second mode. It can be observed that the interfacial imperfections exert a greater influence on the modal frequency at the small wavenumbers. Furthermore, all the curves seem to approach asymptotic values when $\gamma \to \infty$. It can be inferred that the asymptote should be the non-dispersive first modes in the cylinder.

THICKNESS EFFECT

For a composite hollow cylinder, the outer tube is expected to functionalize as the coating layer to avoid the corrosion of air and water. Its thickness may experience a constant decrease in the service process. Therefore, this study further investigates the thickness effect on the torsional wave features considering imperfect interface conditions.

To quantify the varying thicknesses, we introduce non-dimensional parameters as

$$\bar{h}=\frac{b-a}{a},\bar{c}=\frac{c}{a},\bar{k}=ka,\bar{k}_j=k_j a,\bar{q}_j=q_j a\,. \tag{22}$$

Thus, Eqs. (13)-(16) can be rewritten as

$$A_1 Z_2(\bar{q}_1\bar{c})+\bar{q}_1^{\,2}B_1 W_2(\bar{q}_1\bar{c})=0 \tag{23}$$

$$A_2 Z_2\left[\bar{q}_2(1+\bar{h})\right]+\left[\bar{q}_2(1+\bar{h})\right]^2 B_2 W_2\left[\bar{q}_2(1+\bar{h})\right]=0 \tag{24}$$

$$(\mu_1/\mu_2)\left[A_1 Z_2(\bar{q}_1)+\bar{q}_1^{\,2}B_1 W_2(\bar{q}_1)\right]-A_2 Z_2(\bar{q}_2)-\left[\bar{q}_2(1+\bar{h})\right]^2 B_2 W_2(\bar{q}_2)=0 \tag{25}$$

$$\begin{aligned}&\left[\bar{q}_1(1+\bar{h})\right]^{-1}A_1\left[Z_1(\bar{q}_1)-\gamma\bar{q}_1 Z_2(\bar{q}_1)\right]-\left[\bar{q}_2(1+\bar{h})\right]^{-1}A_2 Z_1(\bar{q}_2)\\&-\left[\bar{q}_1(1+\bar{h})\right]^{-1}(\bar{q}_1)^2 B_1\left[\gamma\bar{q}_1 W_2(\bar{q}_1)-W_1(\bar{q}_1)\right]-B_2\left[\bar{q}_2(1+\bar{h})\right]W_1(\bar{q}_2)=0\end{aligned}\,. \tag{26}$$

Using Taylor series expansions at $\bar{h}=0$ up to the first order by Mathematica as,

$$Z_2\left[\bar{q}_2(1+\bar{h})\right]=\begin{cases}J_2\left[\bar{q}_2(1+\bar{h})\right]\approx J_2(\bar{q}_2)+\left[2J_2(\bar{q}_2)-\bar{q}_2 J_3(\bar{q}_2)\right]\bar{h}, k_j^2\geq k^2\\ I_2\left[\bar{q}_2(1+\bar{h})\right]\approx I_2(\bar{q}_2)+\left[2I_2(\bar{q}_2)+\bar{q}_2 I_3(\bar{q}_2)\right]\bar{h}, k_j^2\leq k^2\end{cases} \tag{27}$$

$$W_2\left[\bar{q}_2(1+\bar{h})\right]=\begin{cases}Y_2\left[\bar{q}_2(1+\bar{h})\right]\approx Y_2(\bar{q}_2)+\left[2Y_2(\bar{q}_2)-\bar{q}_2 Y_3(\bar{q}_2)\right]\bar{h}, k_j^2\geq k^2\\ K_2\left[\bar{q}_2(1+\bar{h})\right]\approx K_2(\bar{q}_2)+\left[2K_2(\bar{q}_2)-\bar{q}_2 K_3(\bar{q}_2)\right]\bar{h}, k_j^2\leq k^2\end{cases} \tag{28}$$

$$(1+\bar{h})^2\approx 1+2\bar{h},(1+\bar{h})^{-1}\approx 1-\bar{h}\,. \tag{29}$$

Therefore, by only retaining the linear terms, Eqs. (24)-(26) can be formulated as

$$\begin{aligned}&A_2\left\{Z_2(\bar{q}_2)+\left[2Z_2(\bar{q}_2)-\bar{q}_2 Z_3(\bar{q}_2)\right]\bar{h}\right\}\\&+\bar{q}_2^{\,2}B_2\left\{W_2(\bar{q}_2)+\left[4W_2(\bar{q}_2)-\bar{q}_2 W_3(\bar{q}_2)\right]\bar{h}\right\}=0\end{aligned} \tag{30}$$

$$(\mu_1/\mu_2)\left[A_1 Z_2(\bar{q}_1)+\bar{q}_1^{\,2}B_1 W_2(\bar{q}_1)\right]-A_2 Z_2(\bar{q}_2)-\bar{q}_2^{\,2}\left(1+2\bar{h}\right)B_2 W_2(\bar{q}_2)=0 \tag{31}$$

$$\begin{aligned}&\bar{q}_1^{\,-1}(1-\bar{h})A_1\left[Z_1(\bar{q}_1)-\gamma\bar{q}_1 Z_2(\bar{q}_1)\right]-\bar{q}_2^{\,-1}(1-\bar{h})A_2 Z_1(\bar{q}_2)\\&-\bar{q}_1^{\,-1}(1-\bar{h})(\bar{q}_1)^2 B_1\left[\gamma\bar{q}_1 W_2(\bar{q}_1)-W_1(\bar{q}_1)\right]-B_2\left[\bar{q}_2(1+\bar{h})\right]W_1(\bar{q}_2)=0\end{aligned}\,. \tag{32}$$

When $\bar{h}\to 0$ (without the outer tube), Eqs. (30)-(32) render

$$A_2 Z_2(\bar{q}_2)+\bar{q}_2^{\,2}B_2 W_2(\bar{q}_2)=0 \tag{33}$$

$$(\mu_1/\mu_2)\left[A_1 Z_2(\bar{q}_1)+\bar{q}_1^{\,2}B_1 W_2(\bar{q}_1)\right]-A_2 Z_2(\bar{q}_2)-\bar{q}_2^{\,2}B_2 W_2(\bar{q}_2)=0 \tag{34}$$

$$\begin{aligned}&\bar{q}_1^{\,-1}A_1\left[Z_1(\bar{q}_1)-\gamma\bar{q}_1 Z_2(\bar{q}_1)\right]-\bar{q}_2^{\,-1}A_2 Z_1(\bar{q}_2)\\&-\bar{q}_1 B_1\left[\gamma\bar{q}_1 W_2(\bar{q}_1)-W_1(\bar{q}_1)\right]-B_2\bar{q}_2 W_1(\bar{q}_2)=0\end{aligned}\,. \tag{35}$$

Therefore, Eqs. (33)-(35) can be utilized to calculate the wave-propagation features in a hollow cylinder without the outer coating layer.

Dispersion Curves with Varying Coating Thicknesses

In order to compare the dispersion curves regarding with various coating thicknesses, three cases are selected, i.e., $\bar{h} \to 0$ (without coating layer case), $\bar{h} = 1/1100$ (reduced coating thickness case), and $\bar{h} = 1/110$ (composite hollow cylinder condition). Figure 5 and Figure 6 show the computational results for the second and third modes, respectively.

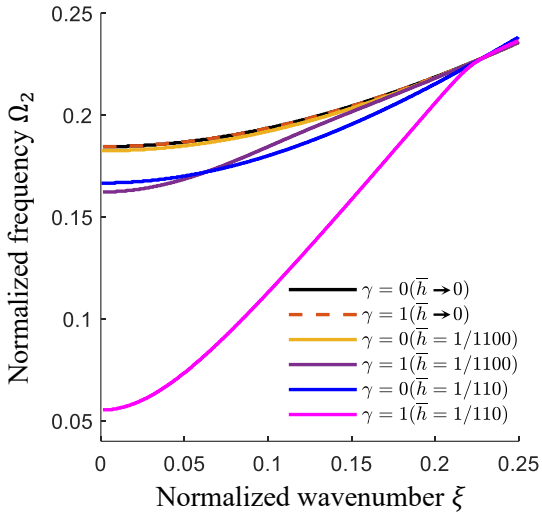

Figure 5. Dispersion curves for the second mode with different coating thicknesses.

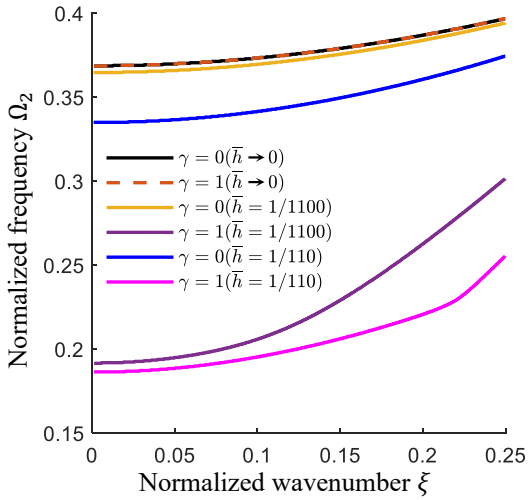

Figure 6. Dispersion curves for the third mode with different coating thicknesses.

It can be noticed that the modal frequency increases with the coating thickness decreasing, especially for the small values of wavenumber. In other words, for the fixed wavenumber, torsional waves in the thicker-coating cylinder would propagate slower than those in the thinner one. Thus, we can take advantage of the changes to wave velocities to predict the variation of the coating thickness. Besides, if a composite hollow cylinder completely loses its outer tube, the wave-propagation features will not

be affected by the interfacial imperfections. This aspect can be reflected on the superposition of the dispersion curves when $\bar{h} \to 0$.

CONCLUDING REMARKS

This paper presented a systematic investigation of torsional wave propagation in a composite hollow cylinder considering imperfect interface conditions. The spring interface compliance was utilized to describe the interface imperfections. It was found that the interfacial imperfections had a great influence on the dispersion curves within the small wavenumber ranges. In addition, the modal frequencies increased with the thickness of the outer tube declined. These wave features may help develop effective NDE and SHM methodologies for the inspection of composite hollow cylinders.

ACKNOWLEDGEMENTS

This research was supported in part by the US Department of Energy through its Nuclear Energy University Programs, DE-NE0008943.

REFERENCES

[1] S. K. Clark, "Torsional Wave Propagation in Hollow Cylindrical Bars," *The Journal of the Acoustical Society of America*, vol. 28, no. 6, pp. 1163-1165, 1956.

[2] A. E. Armenakas, "Torsional Waves in Composite Rods," *The Journal of the Acoustical Society of America*, no. 3, pp. 439-446, 1965.

[3] A. E. Armenakas, "Propagation of Harmonic Waves in Composite Circular-Cylindrical Rods," *The Journal of the Acoustical Society of America*, vol. 47, no. 3B, pp. 822-837, 1970.

[4] M. J. S. Lowe, D. N. Alleyne and P. Cawley, "Defect detection in pipes using guided waves," *Ultrasonics*, vol. 36, no. 1-5, pp. 147-154, 1998.

[5] J. R. Berger, P. A. Martin and S. J. McCaffery, "Time-harmonic torsional waves in a composite cylinder with an imperfect interface," *J Acoust Soc Am*, vol. 107, no. 3, pp. 1161-1167, 2000.

[6] T. Kepceler, "Torsional wave dispersion relations in a pre-stressed bi-material compounded cylinder with an imperfect interface," *Applied Mathematical Modelling*, vol. 34, no. 12, pp. 4058-4073, 2010.

[7] A. Ozturk, "Propagation of torsional waves in pre-stretched composite cylinder with an imperfect interface," in *Turkish Physical Society 32nd International Physics Congress*, Bodrum, Turkey, 2017.

[8] L. Xu, H. Fan and Y. Zhou, "Torsional wave in a circular micro-tube with clogging attached to the inner surface," *Acta Mechanica Solida Sinica*, vol. 30, no. 3, pp. 299-305, 2017.

[9] P. A. Martin, "Boundary integral equations for the scattering of elastic waves by elastic inclusions with thin interface layers," *Journal of Nondestructive Evaluation*, vol. 11, no. 3-4, pp. 167-174, 1992.